Journal of Structural Geology, Vol. 3, No. 1, pp. 77 to 87, 1981
Printed in Great Britain

0191-8141/81/010077-10 $02.00/0

Mineral reactions participating in intragranular fracture propagation: implications for stress corrosion cracking

R. KERRICH, T. E. LA TOUR and R. L. BARNETT

Department of Geology, University of Western Ontario,
London, Ontario, Canada, N6A 5B7

(*Received* 15 *October* 1980; *accepted in revised form* 5 *January* 1981)

Abstract—Two examples of mineral reactions accompanying intragranular fracturing of silicates are described from amphibolites at the Grenville front, Coniston, Ontario, and a granodiorite within the Miéville shear zone, Switzerland. At these localities coarse grained (> 1 mm) hornblende and biotite respectively have undergone initial deformation by intense transgranular fracturing. The ambient temperature of deformation is estimated at 400–500°C for the amphibolites, and 250–300°C for the granodiorite.

Fracture intensity within hornblende increases with progressive deformation until fractures coalesce and grains lose cohesion. Fractures are occupied by hornblende in close optical continuity with the parent grain, and typically contain median sutures decorated by arrays of solid inclusions. Relative to the parent grain, hornblende in fractures is depleted in Ti, Al, plus K, and enriched in Mg. Given the preferential partitioning of Mg, Al^{VI} and Ti into the M2 site of calcic amphiboles, the decrease of Ti and Al^{VI} in the host-to-crack transition is consistent with the corresponding increase of the $Mg/(Mg + Fe^{2+})$ ratio.

Fractures within biotite are bounded by an envelope of paler brown biotite which corresponds to a decrease of Ti and increase of Fe + Mg relative to regions unaffected by cracking. Fractures are occupied by secondary ilmenite, low-Ti biotite and high-Ti muscovite. Ti and Al do not vary significantly as a function of Mg/(Fe + Mg) in the host-to-crack transition, as anticipated from the approximately equal partitioning of these two cations into the M1 and M2 octahedral cation sites. The direct relationship of the mineral reactions to the fractures is taken as evidence for the participation of the reactions in crack propagation. These features may thus represent examples of natural stress corrosion cracking.

INTRODUCTION

FRACTURES may propagate by a number of alternative micromechanisms which include brittle rupture, stress corrosion and ductile faulting. Stress corrosion cracking involves chemical reactions of the host material at, or in the vicinity of, the crack tip, such that the energy requirements for crack propagation are reduced (Anderson & Grew 1977). Slow, stable crack growth by stress corrosion will proceed above a threshold stress for catalysing the reaction, but below the critical stress intensity for fast irreversible brittle rupture in 'Griffith cracks'. In this paper we describe transgranular fractures in silicate minerals from deformed rocks where chemical reactions of the host grains are apparently catalysed at fracture tips, and thereby participate in the process of crack propagation. These fractures may thus represent natural examples of stress corrosion cracks in rocks.

The subject of stress corrosion cracking has been reviewed by Anderson & Grew (1977). Slow crack growth at sub-critical stress intensities has been extensively studied in metals, ceramics, and glasses (Evans 1974, McKinnis 1978, Wiederhorn 1978, Michalske *et al.* 1978, Yaholm 1979). A theoretical treatment of sub-critical crack growth is given by Stevens *et al.* (1974), and Puls *et al.* (1974). Fracture mechanism maps for FCC metals have been constructed by Ashby *et al.* (1979).

Time dependent cracking has been experimentally demonstrated in quartz by Scholz (1968), Martin (1972), and Atkinson (1979); and in rocks by Atkinson (1980), Dunning (1979), Wilkins (1979), and Peck (1980). Slow growth of flaws is implicated in a number of geological phenomena such as prefaulting dilatancy and magmatic intrusion (Anderson & Grew 1977); and Greenwood (1978) and Gorman (1980) discuss fracturing during ductile creep of rocks. However, stress corrosion cracking has not been extensively described from naturally deformed rocks.

GEOLOGICAL SETTING

Naturally deformed rocks in which pervasive transgranular fracturing of silicate minerals is an important feature, are described from two localities — amphibolites involved in the Grenville Front thrust, and a granodiorite transected by a major shear zone at Miéville, Switzerland.

Deformed amphibolites from Coniston

The amphibolites examined in this study are within migmatitic layered gneisses of the Grenville structural province, located 150 m southeast of the Grenville front, at Coniston, Ontario, Canada (Fig. 1). During pre- or early Grenville time the rocks underwent prograde regional metamorphism to staurolite grade with accompanying development of a penetrative schistosity. Subsequently, in late Grenville time (~ 1 Ga) a mylonitic fabric characteristic of intense deformation along the Grenville front was superimposed on earlier structures (Wynne-Edwards 1972).

In the amphibolites, microstructures associated with

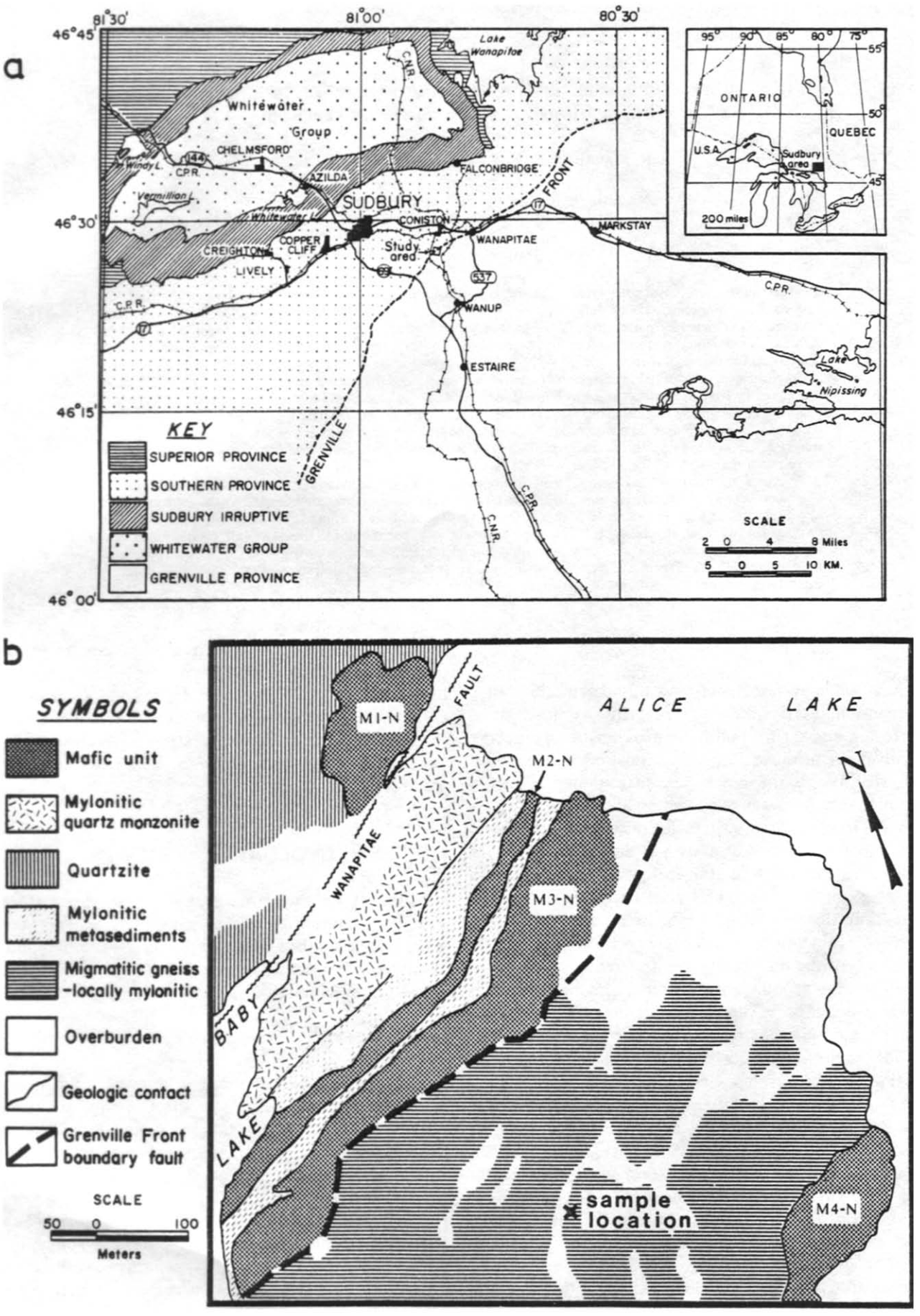

Fig. 1. Simplified geological map illustrating the disposition of deformed amphibolites in proximity to the Grenville Front, Ontario. (a) Generalised geology of the Sudbury area. (b) Disposition of units at the sampling locality.

the latter event are generally brittle fracturing of hornblende (Allison & LaTour 1977), and dynamic recrystallisation of plagioclase and quartz. The metamorphism accompanying the mylonitic deformation was retrograde, producing Ti- and Al-poor calcic amphibole (and locally chlorite plus sphene) from hornblende; and albite plus clinozoisite from oligoclase. Within interlayered pelites garnet has been largely converted to chlorite plus quartz. These reactions indicate that the temperature during mylonitic deformation was between 400 and 500°C (Winkler 1974, p. 183 and pp. 165–166 respectively).

Sheared granodiorite— Miéville

At Miéville, Switzerland, granodiorite basement rocks of the Aiguilles Rouges Massif are deformed into mylonites within a major subvertical shear zone (Reinhard & Preiswerk 1927, Steck & Vocat 1973). The granodiorite is composed of orthoclase + oligoclase + biotite + quartz. At low states of deformation in the margins of the shear zone feldspar porphyroclasts and biotite underwent grain size reduction by pervasive transgranular fracturing. The ambient temperature during deformation is estimated at 250–300°C from mineralogical criteria, combined with oxygen isotope and fluid inclusion thermometry (Kerrich *et al.* 1980).

ANALYTICAL METHODS

Analyses of mineral chemical composition were performed on a three spectrometer MAC 400 electron microprobe incorporating a KRISEL automation system (Finger & Hadidiacos 1972), and utilising appropriate natural minerals for calibration standards. Operating conditions were 15 kv accelerating voltage and 0.03 μamp sample current. The electron beam was enlarged to minimise possible breakdown of fine-grained hydrous silicates. Data reduction was by an on-line PDP-11/05 computer using the MAGIC IV data reduction programme. The structural formulae of amphiboles were calculated on the basis of 23 oxygens using the programme AMPHIBOLE (Papike *et al.* 1974); those of biotite and muscovite were calculated on the basis of 22 oxygens using the programme SUPREC written by Dr. J. C. Rucklidge of the University of Toronto.

FRACTURING OF AMPHIBOLE

At low states of strain, hornblendes in the amphibolites at Coniston exhibit transgranular fracturing, the intensity of which increases with progressive deformation until the fractures coalesce and the grains lose cohesion. The fractures are of three types: (1) cracks occupied by secondary hornblende; (2) cracks occupied by orthoclase feldspar and (3) cracks containing chlorite + epidote + sphene. All of the fractures appear to be tensile in character, and to have developed essentially contemporaneously. Where cross-cutting relationships were observed, type 1 generally predates the other fractures present. There is little evidence for displacements along fractures, but fibrous chlorite may bridge fracture boundaries. The following discussion is concerned with those cracks occupied by secondary hornblende (Fig. 2).

Hornblende within fractures is in close optical continuity with the host grain. A median suture, marked by a zone of solid inclusions ($\sim 3\,\mu$m in size), is typically present along the centre line. Where fractures widen, hornblende may be replaced by orthoclase feldspar.

Microprobe analyses of the chemical composition of the host grain and secondary minerals occupying a crack, together with a schematic diagram illustrating the sites of analysis, are contained in Tables 2 and 3 of the Appendix. Average host and crack compositions are given in Table 1 and plotted in Fig. 3. Inspection of the data reveals that relative to the host grain of hornblende, cracks are depleted in TiO_2, Al_2O_3 and K_2O, but are enriched in MgO. The direct relationship of the chemical reaction to the fracture, and its inception at the crack front, is taken as evidence for participation of the reaction in crack propagation. These intragranular fractures may therefore be examples of natural stress corrosion cracking. The nature of these microstructures constrasts with brittle transgranular fracturing of hornblende in which no mineralogical change accompanies cracking in nearby deformed amphibolites previously described by Allison & La Tour (1977).

The internal chemical variation in both the host grain and the zone of stress corrosion is substantial (Fig. 3 and Appendix Tables 1, 2 and 3). Total aluminium exhibits a continuous variation from host to crack and an antipathetic relationship with the $Mg/(Mg + Fe^{2+})$ ratio. Titanium variation relative to this ratio is discontinuous and less regular. La Tour (1979, p. 228) showed that variability in Ti contents of the Coniston amphiboles is independent of whole-rock Ti contents; hence, Ti concentration in the amphiboles is likely to be some function of the physical conditions during crystallization (cf. Raase 1974). The wide variation in Ti and Al in the host grain is therefore an indication of the general degradation of the amphibole during conditions of lower metamorphic grade; and the abrupt change in colour and Ti contents from host to crack is due to localized more nearly complete degradation, possibly catalysed by increase of the stress intensity at fracture tips.

Utilising the average host and crack compositions, a two-way mass balance calculation was performed according to the method of Gresens (1966). The results suggest an approximately constant volume reaction of the host hornblende to secondary hornblende within the crack, as defined by essentially isochemical behaviour of SiO_2, FeO, CaO and MnO. The absence of a Ti phase such as ilmenite or sphene within the crack signifies transport of components out of the grain (cf. Chayes 1954). This contrasts with the chlorite plus sphene association found in type 3 fractures as mentioned above.

Calcic amphiboles possess four distinct octahedrally coordinated cation sites M1, M2, M3 and M4. Site M4 is

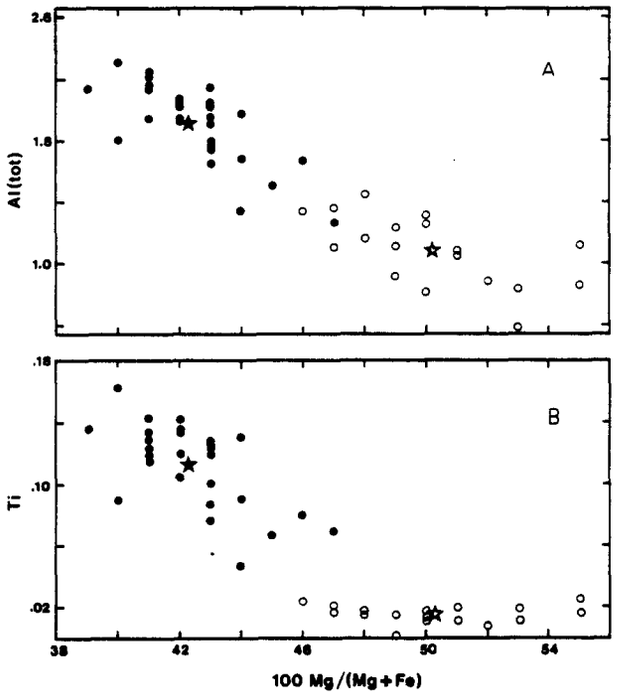

Fig. 3. Variation of total aluminum (A) and titanium (B) with 100 Mg/(Mg + Fe). (Fe total). Solid symbols, host grain; open symbols, crack; dots, individual spot analyses; stars, averages. Values are number of atoms per formula unit (see Appendix Tables 1, 2 and 3).

occupied almost exclusively by Ca and to a lesser extent Na. The other three sites are occupied principally by Fe^{2+} and Mg but also may contain Al^{VI}, Ti, Mn and Fe^{3+}. Ti and Al^{VI} are preferentially partitioned into the M2 site (Kretz 1978), and this site also has the greatest preference for Mg (or least preference for Fe^{2+}, Bancroft & Brown 1975). According to Kretz (1978)

$$(Mg/Mg + Fe^{2+})_{M2} = 2.53\,(Mg/Mg + Fe^{2+})_{(M1+M3)};$$

consequently, with decreasing Ti or Al^{VI} in the amphibole, the Mg content and $Mg/Mg + Fe^{2+}$ ratio should become increasingly dominated by these parameters in the M2 site and thus increase overall. This is observed in the transition from host to crack (or rim) in sample 6477 (Appendix Tables 1, 2 and 3).

A generalized reaction during cracking of the hornblende is as follows:

average host amphibole

$$(Ca_{1.815}Na_{0.390}K_{0.160})(Mg_{1.825}Fe^{2+}_{2.490}Fe^{3+}_{0.043}Mn_{0.045}Ti_{0.113}Al^{VI}_{0.613})(Si_{6.680}Al^{IV}_{1.320})O_{22}(OH)_2 + 0.103\,CaO + 0.446\,MgO + 0.0725\,Fe_2O_3 + 0.546\,SiO_2$$

$$\rightleftarrows$$

average crack amphibole

$$(Ca_{1.918}Na_{0.202}K_{0.049})(Mg_{2.271}Fe^{2+}_{2.255}Fe^{3+}_{0.188}Mn_{0.040}Ti_{0.016}Al^{VI}_{0.309})(Si_{7.226}Al^{IV}_{0.774})O_{22}(OH)_2 + 0.425\,Al_2O_3 + 0.097\,TiO_2 + 0.235\,FeO + 0.005\,MnO + 0.094\,Na_2O + 0.0165\,K_2O.$$

(Note: slight adjustments were made so as to yield exactly 46.000 positive charges in each amphibole, excluding H^+ in OH radicals.)

Most of the amphiboles contained in the amphibolites of the layered gneisses possess pale green rims which are optically distinguishable from their dark green cores. The rims and cores are in crystallographic continuity, and the contact between them is sharp. Microprobe analyses indicate that relative to the cores, the rims are depleted in TiO_2, Al_2O_3, alkalis and FeO, and enriched in MgO (La Tour 1979, ch. 7). Hence amphibole in the type 1 cracks has a colour and chemical composition close to that of the rims, and some cracks appear to have propagated from rims towards the interior of grains (Fig. 2).

The core–rim–crack textural relationship and variation in composition may be explained by one of the following.

(i) The rims represent compositional zones which formed during continuous amphibole growth at changing P–T conditions, and the sharp contact is a manifestation of a miscibility gap in the calcic amphiboles.

(ii) The rims constitute a retrograde reaction product of pre-existing amphibole, and the sharp contact is evidence of a miscibility gap.

(iii) The rims formed by mimetic replacement of pre-existing amphibole during retrograde metamorphism, and the sharp contact represents a migratory reaction front which is unrelated to any inferred miscibility gap.

Alternative (iii) above is favoured in the present case for a number of reasons.

(a) Several workers have recently shown that sharp contacts are not incompatible with replacement origins (e.g. Fleet & Barnett 1978, Grapes & Graham 1978, Thomson *et al.* 1980).

(b) Most proposed miscibility gaps involve amphiboles with widely disparate Al contents, in contrast to the present case (e.g. Cooper 1972, Brady 1974, Hietanen 1974).

(c) A miscibility gap implies equilibrium at some T and P between two coexisting amphiboles of essentially fixed composition, in contrast to the large intragranular variation in composition shown by the Coniston amphiboles (Fig. 4).

(d) Rimming of amphiboles in some of the Coniston rocks is spatially restricted to μm-size zones between Ti- and Al-rich amphibole and mm-size epidote veins which post-date the schistosity and transect the entire hand specimen.

The amphibole associated with the stress corrosion crack described here is an optical and crystallographic continuation of one of these rims which has locally

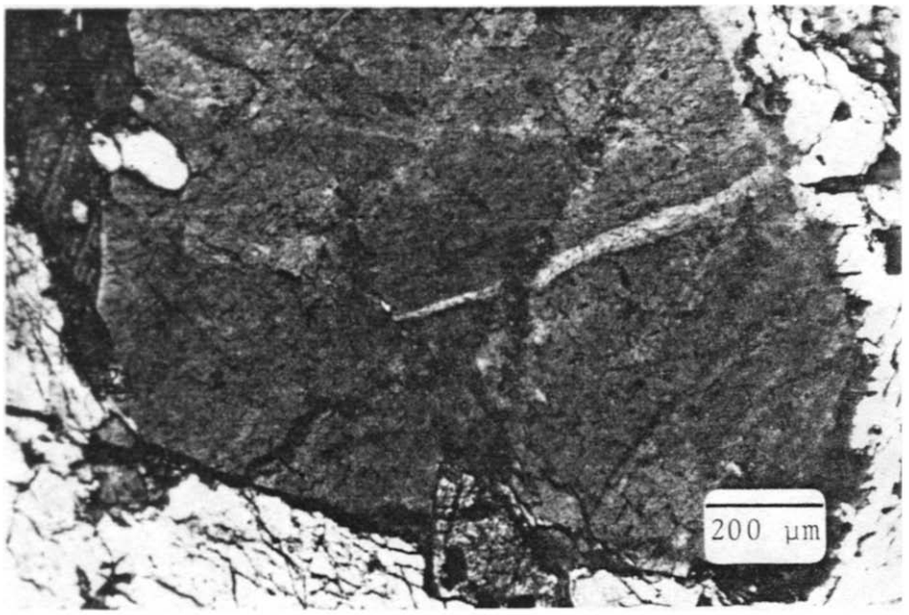

Fig. 2. Photomicrograph portraying the onset of intragranular fracturing in hornblende at low states of deformation in the amphibolites. Reaction of the parent hornblende to an Al and Ti depleted variety within the crack.

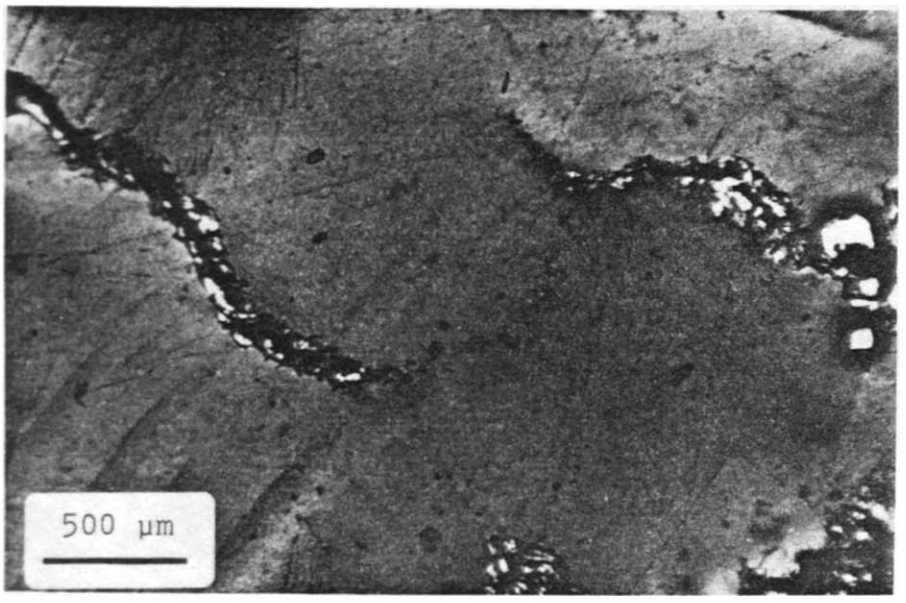

Fig. 4. Photomicrograph of intragranular fracture in biotite (cross polarisers). Fractures are occupied by secondary ilmenite + muscovite + low Ti biotite. Note the pale envelope surrounding the fractures, and the absence of displacement as indicated by the registration of some inclusion trails across the fractures.

penetrated deep into the interior of the host grain. This relationship is incompatible with metamorphic growth zoning, but is easily explained in terms of retrograde alteration (see (iii) above). In addition, the chemical continuity of the rim and the corrosion crack has been verified by microprobe analyses (see Appendix Table 3). The pale green amphibole of the stress corrosion crack and that of the amphibole rim are therefore both products of the same retrograde metamorphic event which accompanied mylonitic deformation in the area (La Tour 1979). It is pertinent that amphibolites which were more intensely deformed possess broken and dismembered amphiboles in which chlorite plus sphene has grown along fractures apparently at the expense of the amphibole (crack type 3). This latter retrogression does not appear to have occurred during initial amphibole fracturing, but was facilitated at a later date by the presence of the fractures together with fluid access.

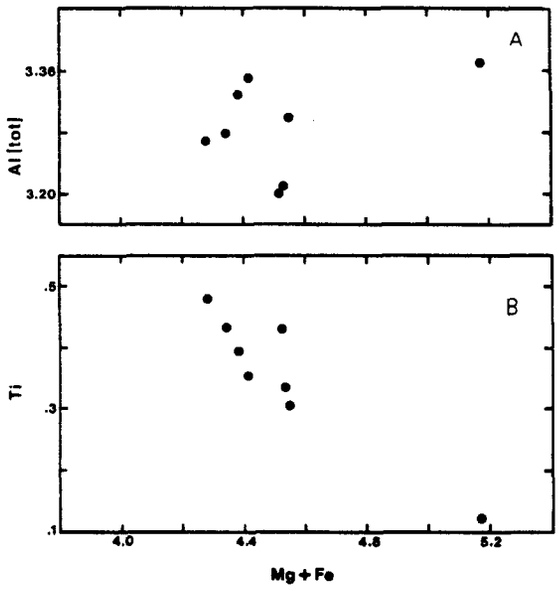

Fig. 5. Variation of total aluminium (A) and titanium (B) with Mg + Fe from the parent biotite into the fracture envelope.

FRACTURING OF BIOTITE

At low states of deformation in the margins of the shear zone at Miéville, feldspars and biotite underwent grain size reduction by intragranular fracturing. The fracture characteristics and mineral reactions accompanying cracking were briefly described by Barnett & Kerrich (1980). The following is a more detailed discussion of the mineral reactions which are believed to participate in crack propagation through biotite. Microprobe analyses of biotite grains and secondary mineral reactants occupying fractures are given in Appendix Table 4.

Grains of biotite have fractures with irregular shapes, which appear not to involve significant displacements as evidenced by the registration of trails of solid inclusions across fractures (Fig. 4). The fractures are bounded by an envelope of paler brown biotite in crystallographic continuity with the host grain, with a width of 80–300 μm: this region corresponds to a decrease of Ti and increase of Fe + Mg relative to the composition of grains in areas unaffected by cracking (Appendix Table 4). Fracture openings are occupied by fine-grained secondary ilmenite, low-Ti biotite, and high-Ti muscovite (Fig. 4). Ilmenite is disposed along the median line of fractures (Fig. 4), and this, together with other microstructures described above, provides evidence for active participation of the mineral reaction in crack propagation. Secondary mineral products are also present in kink band walls, and at grain boundaries where the parent biotites have recrystallised, but do not occur at grain boundaries in undeformed rocks.

Biotite possesses two octahedral cation sites, M1 and M2, which are similar to sites M1 and M3 in amphibole (Kretz 1978). This implies that the affinity of octahedrally coordinated cations in biotite for one site over the other is likely to be small. This has been supported by Annersten (1974) who reported the preferential partitioning of Fe^{2+} into the M2 sites, and Mg into the M1 site to be only slight in biotites. The similarity of the two sites has also been verified by Bancroft & Brown (1975) who determined the occupation of both sites by Fe^{2+} and Fe^{3+} to be essentially the same. Hence, it is reasonable to assume that partitioning of Ti and Al into the two sites would be approximately equal as well.

Plots of Ti or total Al with Mg/(Mg + Fe) (not shown) do not exhibit systematic variation, an observation expected from the arguments presented above. However, Ti bears an antipathetic relationship with Mg + Fe (Fig. 5), presumably reflecting competition for the octahedral sites. On the other hand, Al values are more scattered with respect to Mg + Fe, but show an overall sympathetic relationship, even though Al is also competing for these sites (Fig. 5). Since the Al^{VI} content of biotites is normally related to the substitution (Mg, Fe)Si $\rightleftarrows$ $Al^{VI}Al^{IV}$, increase in Mg + Fe would be expected to be accompanied by a decrease in total Al, not an increase. A plausible explanation appears to be that a different substitution involving Ti is an integral aspect of the biotite compositions. For example, a substitution of the type $3Ti1[\ ] \rightleftarrows 4Al^{VI}$ may be involved in which Mg and Fe play no part. Alternatively, the substitution $3Ti2[\ ] \rightleftarrows 3(Mg, Fe)\ 2Al^{VI}$ would cause trends consistent with those in Fig. 5. (In this notation 1[ ] or 2[ ] indicates the number of available sites.)

A generalised reaction during cracking of the biotite is as follows:

average host biotite

$$(K_{1.848}Na_{0.039})(Fe_{2.660}Mg_{1.622}$$
$$Mn_{0.031}Ti_{0.481}Al^{VI}_{0.707})$$
$$(Al^{IV}_{2.563}Si_{5.438})O_{20}(OH)_4$$
$$+ 0.005\,K_2O + 0.215\,FeO + 0.175\,MgO$$
$$+ 0.009\,MnO + 0.006\,SiO_2$$

$\rightleftarrows$

secondary biotite in crack

$$(K_{1.858}Na_{0.006})(Fe_{2.875}Mg_{1.797}$$
$$Mn_{0.040}Ti_{0.335}Al^{VI}_{0.650})$$
$$(Al^{IV}_{2.559}Si_{5.444})O_{20}(OH)_4$$
$$+ 0.0165\,Na_2O + 0.146\,TiO_2 + 0.0305\,Al_2O_3.$$

(Note: Adjustments were made so as to yield exactly 44.000 positive charges in each biotite excluding H^+ in OH radical.)

DISCUSSION

In the consideration of mineral alteration along fractures it is difficult to establish unequivocally whether the observed reactions proceeded during crack propagation. An alternative is that the fractures grew in the absence of stress corrosion and subsequently provided pathways for the enhanced access of reactants, such as water, facilitating alteration of the parent grain.

For the two examples of grain fracturing examined in this study, reaction of the parent grain appears to be initiated at, or in advance of crack tips. This feature, coupled with the presence of secondary mineral products plus solid inclusions of the host grain in arrays along median sutures, in which the local chemical system is essentially closed, may provide diagnostic criteria for participation of the reaction in crack propagation. In addition, the cracks are exclusively intragranular, with the reactions accompanying cracking not involving net hydration. This contrasts with late fractures that transect many grains, and which contain hydrated, lower grade products of the host amphibole, such as chlorite + epidote.

The cracking described in both hornblende and biotite is most pronounced at low states of deformation. With progressive strain the intragranular fractures coalesce, and the grain loses cohesion resulting in a decrease in grain size by about a factor of ten. At higher states of deformation further grain size reduction is accomplished by dynamic recrystallisation.

Acknowledgements — The authors express their thanks to M. E. Fleet and two anonymous reviewers for their incisive criticisms of an earlier version of the manuscript, and for suggesting improvements. We are grateful to Professors S. Ayrton and J. Starkey for the use of their material collected from Miéville. Analytical assistance was kindly provided by J. Forth. R. Kerrich and T. La Tour received support from the National Research Council of Canada.

REFERENCES

Allison, I. & La Tour, T. E. 1977. Brittle deformation of hornblende in a mylonite: a direct geometrical analogue of ductile deformation by translation gliding. *Can. J. Earth Sci.* **14**, 1953–1958.

Anderson, O. L. & Grew, P. C. 1977. Stress corrosion theory of crack propagation with application to geophysics. *Rev. Geophys. Space Phys.* **15**, 77–104.

Annersten, H. 1974. Mössbauer studies of natural biotite. *Am. Miner.* **59**, 143–151.

Ashby, M. F., Gandhi, C. & Taplin, D. M. R. 1979. Fracture-mechanism maps and their construction for FCC metals and alloys. *Acta metall.* **27**, 699–729.

Atkinson, B. K. 1979. A fracture mechanics study of subcritical tensile cracking of quartz in wet environments. *Pageoph.* **117**, 1011–1024.

Atkinson, B. K. 1980. Stress corrosion and the rate-dependent tensile failure of a fine-grained quartz rock. *Tectonophysics* **65**, 281–291.

Barnett, R. L. & Kerrich, R. 1980. Stress corrosion cracking of biotite and feldspar. *Nature, Lond.* **283**, 185–187.

Bancroft, G. M. & Brown, J. R. 1975. A Mössbauer study of coexisting hornblendes and biotites. *Am. Miner.* **60**, 265–272.

Brady, J. B. 1974. Coexisting actinolite and hornblende from west-central New Hampshire. *Am. Miner.* **59**, 529–535.

Chayes, F. 1954. Potash feldspar as a by-product of the biotite–chlorite transformation. *J. Geol.* **62**, 75–82.

Cooper, A. F. 1972. Progressive metamorphism of metabasic rocks from the Haast Schist Group of Southern New Zealand. *J. Petrol.* **13**, 457–492.

Dunning, J. D. 1979. Chemomechanical weakening of synthetic quartz and sandstone in the presence of surfectants. *Geol. Soc. Am. Abs. with Progs.* **11**, no. 7, 417.

Evans, A. G. 1974. Slow crack growth in brittle materials under dynamic loading conditions. *Int. J. Fract.* **10**, 251–259.

Finger, L. W. & Hadidiacos, C. G. 1972. Electron microprobe automation. *Annu. Rep. geophys. Lab. Carnegie Inst. Wash.* **71**, 598–600.

Fleet, M. E. & Barnett, R. L. 1978. Al^{IV}/Al^{VI} partitioning in calciferous amphiboles from the Frood Mine, Sudbury, Ontario, *Can. Mineralogist* **16**, 527–532.

Gorman, B. E. 1980. A model of flow and fracture in plagioclase: examples from shear zones, Fiskenaesset Complex, West Greenland. Unpublished Ph.D. thesis, University of Western Ontario.

Grapes, R. H. & Graham, C. M. 1978. The actinolite–hornblende series in metabasites and the so-called miscibility gap: a review. *Lithos.* **11**, 85–97.

Greenwood, G. W. 1978. Fracture during creep. *Phil. Trans. R. Soc.* **A288**, 213–227.

Gresens, R. L. 1966. Composition-volume relations of metasomatism. *Chem. Geol.* **2**, 47–65.

Hietanen, A. 1974. Amphibole pairs, epidote minerals, chlorite and plagioclase in metamorphic rocks, Northern Sierra Nevada, California. *Am. Miner.* **59**, 22–40.

Kerrich, R., Allison, I., Barnett, R. L., Moss, S. & Starkey, J. 1980. Microstructural and chemical transformations accompanying deformation of granite in a shear zone at Miéville, Switzerland; with implications for stress corrosion cracking and superplastic flow. *Contr. Miner. Petrol.* **73**, 221–242.

Kretz, R. 1978. Distribution of Mg, Fe^{2+}, and Mn in some calcic pyroxene-hornblende-biotite-garnet gneisses and amphibolites from the Grenville province. *J. Geol.* **86**, 599–620.

La Tour, T. E. 1979. The nature and origin of the Grenville front near Coniston, Ontario: a reinterpretation. Unpublished Ph.D. thesis, University of Western Ontario.

Martin, R. J. 1972. Time-dependent crack growth in quartz and its application to the creep of rocks. *J. geophys. Res.* **77**, 1407–1419.

McKinnis, C. L. 1978. Stress corrosion mechanisms in E-glass fiber. In: *Fracture Mechanics of Ceramics*, 4. (edited by Bradt, R. C., Hasselman, D. P. H. & Lange, F. F.) Plenum Press, New York, 581–596.

Michalske, T. A., Varnes, J. R. & Frechette, V. D. 1978. Growth of cracks partially filled with water. In: *Fracture Mechanics of Ceramics*, 4. (edited by Bradt, R. C., Hasselman, D. P. H. & Lange, F. F.) Plenum Press, New York, 639–650.

Papike, J. J., Cameron, K. L. & Baldwin, K. 1974. Amphiboles and pyroxenes: characterizations of other than quadrilateral components and estimates of ferric iron from microprobe data. *Geol. Soc. Am. Abs. with Progs.* **6**, 1053–1054.

Peck, L. 1980. Stress corrosion cracking of quartzite. *Eos.* **61**, 261.

Puls, D. M., Dutton, R. & Stevens, R. N. 1974. The chemical stress applied to creep and fracture theories — II. Application to the growth of subcritical Griffith cracks. *Acta metall.* **22**, 639–647.

Raase, P. 1974. Al and Ti contents of hornblende, indicators of pressure and temperature of regional metamorphism. *Contr. Miner. Petrol.* **45**, 231–236.

Reinhard, M. & Preiswerk, H. 1927. Uber granitmylonite im Aiguilles-Rouges-Massiv (westliche Wallis). *Verh. naturf. Ges. Basel* **38**, 188–200.

Scholz, C. H. 1968. Mechanism of creep in brittle rock. *J. geophys. Res.* **73**, 3295–3302.

Steck, A. & Vocat, D. 1973. Zur mineralogie der granitmylonite von Miéville, Aiguilles-Rouges-Massiv. *Bull. Soc. Suisse Min. Pet.* **53**, 474–477.

Stevens, R. N., Dutton, R. & Puls, M. P. 1974. The chemical stress applied to creep and fracture theories — I. A general approach. *Acta metall.* **22**, 629–638.

Thomson, M. L., Fleet, M. E. & Barnett, R. L. 1980. Coexisting

amphiboles in metamorphosed peridotite from Renzy Lake, southwestern Quebec (abs.). *Geol. Ass. Can. Ann. Meet. Prog. with Abs.* **5**, 84.

Wiederhorn, S. M. 1978. Mechanisms of subcritical crack growth in glass. In: *Fracture Mechanics of Ceramics*, 4. (edited by Bradt, R. C., Hasselman, D. P. H. & Lange, F. F.) Plenum Press, New York, 549–580.

Wilkins, B. J. S. 1979. A study of slow crack growth and its application to nuclear waste disposal in hard rock. *Atomic Energy of Canada Ltd. AECL* 6423.

Winkler, H. G. F. 1974. *Petrogenesis of Metamorphic Rocks.* Springer Verlag, New York.

Wynne-Edwards, H. R. 1972. The Grenville province. In: *Variations in Tectonic Styles in Canada.* (edited by Price, R. A. & Douglas, R. J. W.) *Spec. Pap. Geol. Ass. Can.* **11**, 263–334.

APPENDIX

Table 1. Average compositions of host amphibole and amphibole within crack

	average host grain		average crack	
SiO_2	44.05	(1.24)	48.47	(1.41)
TiO_2	0.99	(0.24)	0.14	(0.05)
Al_2O_3	10.82	(1.44)	6.16	(1.27)
Fe_2O_3	0.38	(0.61)	1.68	(2.00)
FeO[1]	19.51	(0.46)	18.09	(1.01)
MnO	0.33	(0.04)	0.32	(0.04)
MgO	8.08	(0.52)	10.22	(0.69)
CaO	11.18	(0.31)	12.01	(0.68)
Na_2O	1.31	(0.23)	0.70	(0.19)
K_2O	0.86	(0.15)	0.26	(0.08)
Total	97.61		98.05	
100 MgO/ (MgO + FeO)[1]	42.3		50.2	
n[2]	31		18	

1 - average of "mid-point" values calculated for each spot analysis.

2 - number of determinations.

The figures in parentheses represent one standard deviation.

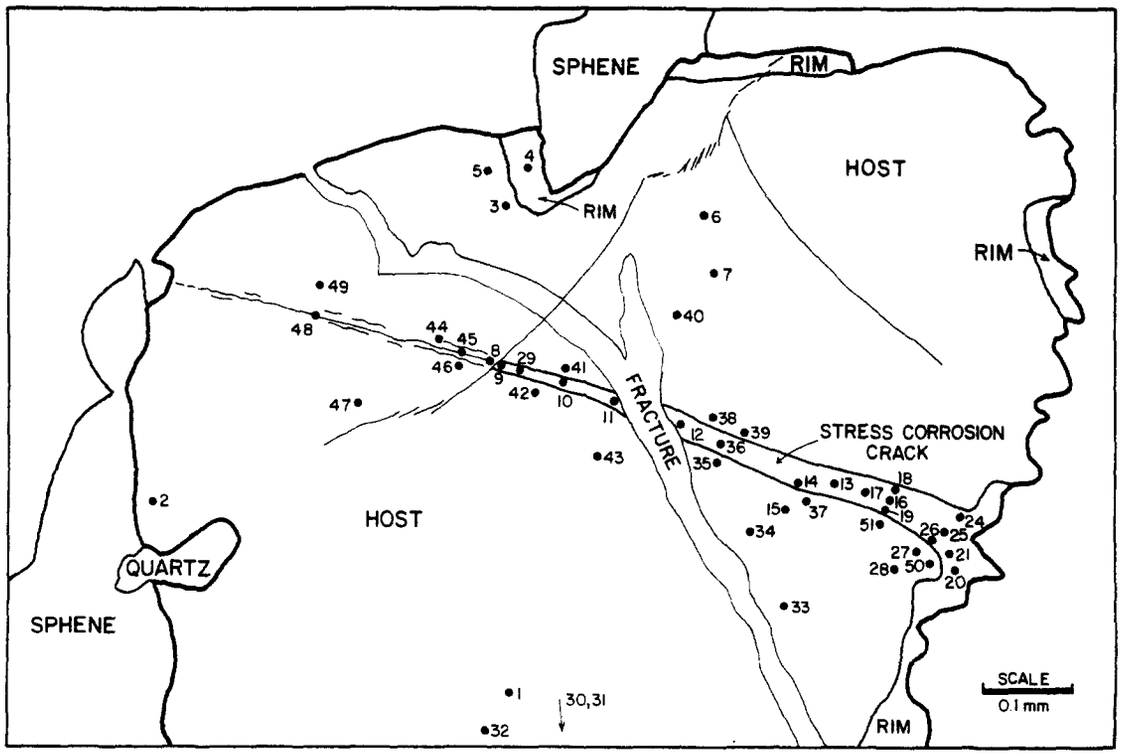

Fig. 6. Location map of microprobe spot analyses of hornblende reported in this study. Compare with photomicrograph (Fig. 2). Numbers correspond to analyses given in Table 3.

Table 2. Spot analyses and structural formulae (23 oxygens) for h
this table is presented in Fig. 6. An average host amphit

	1	2	3	5	6	7	8	15	27	28	30	31	32	33	3
SiO_2	45.42	46.40	44.96	44.83	43.45	43.13	42.84	42.67	41.51	42.41	45.47	45.02	44.03	43.60	43.
TiO_2	0.71	0.60	0.68	0.77	1.03	1.15	1.04	1.08	1.42	1.10	0.41	0.79	1.17	1.26	1.
Al_2O_3	9.40	7.11	10.00	9.79	10.74	11.00	11.29	11.23	12.70	12.13	7.43	9.35	10.93	12.25	11.
Fe_2O^1	1.39	1.82	1.48	0.37	0.00	1.26	0.44	0.72	0.00	1.82	1.28	0.00	0.00	0.00	0.
FeO	19.16	18.70	19.90	20.26	19.35	18.93	19.60	19.28	19.43	19.80	19.55	19.95	20.14	19.31	19.
MnO	0.32	0.33	0.42	0.38	0.40	0.34	0.37	0.40	0.28	0.32	0.34	0.33	0.37	0.29	0.
MgO	9.04	9.31	8.32	8.58	8.13	8.25	7.86	8.29	7.30	8.45	8.71	9.66	8.27	7.93	7.
CaO	11.32	11.45	11.69	11.40	11.59	11.61	11.46	11.34	11.59	10.88	11.66	10.61	10.52	11.28	10.
Na_2O	0.89	0.58	1.11	1.30	1.31	1.19	1.25	1.39	1.73	1.61	1.05	1.31	1.34	1.49	1.
K_2O	0.69	0.52	0.77	0.76	0.86	0.89	0.93	1.05	1.15	1.09	0.63	0.75	0.86	0.98	1.
total	98.34	96.82	99.33	98.44	96.86	97.75	97.08	97.45	97.11	99.61	96.53	96.77	97.63	98.39	97.
Si	6.815	7.054	6.724	6.759	6.648	6.551	6.560	6.516	6.373	6.362	6.987	6.869	6.673	6.549	6.
Al	1.185	.946	1.276	1.241	1.352	1.449	1.440	1.484	1.627	1.638	1.013	1.131	1.327	1.451	1.
Al	.477	.328	.487	.499	.586	.520	.597	.537	.672	.507	.333	.551	.626	.718	.
Ti	.080	.069	.077	.087	.119	.131	.120	.124	.164	.124	.047	.091	.133	.142	.
Fe^{3+}	.157	.209	.167	.042	.000	.144	.051	.083	.000	.205	.148	.000	.000	.000	.
Fe^{2+}	2.404	2.378	2.488	2.554	2.476	2.404	2.510	2.462	2.495	2.485	2.512	2.546	2.553	2.426	2.
Mn	.041	.043	.053	.049	.052	.044	.048	.052	.036	.041	.044	.043	.048	.037	.
Mg	2.021	2.109	1.854	1.928	1.854	1.867	1.794	1.887	1.670	1.889	1.995	1.969	1.868	1.775	1.
Ca	1.820	1.865	1.873	1.842	1.900	1.889	1.880	1.855	1.907	1.749	1.920	1.735	1.709	1.815	1.
Na	.259	.171	.322	.380	.389	.350	.371	.412	.515	.468	.313	.388	.394	.434	.
K	.132	.101	.147	.146	.168	.173	.182	.205	.225	.209	.124	.146	.166	.188	.

Table 3. Spot analyses and structural formulae (23 oxygens) for amphibole associated with crack. A location map of the microprobe spot analyses compiled in this table is presented in Fig. 2. An average crack amphibole composition derived from these data is given in Table 1

	4	9	10	11	12	13	14	16	17	18	19	20	21	24	25	26	29	36
SiO_2	47.89	47.96	49.87	48.48	50.17	48.73	46.38	50.05	48.58	50.91	47.90	45.10	49.05	48.11	48.14	47.13	48.45	49.63
TiO_2	0.15	0.19	0.23	0.07	0.10	0.13	0.13	0.09	0.10	0.17	0.17	0.11	0.15	0.15	0.13	0.21	0.14	0.01
Al_2O_3	7.20	7.79	4.94	5.00	4.78	6.37	8.13	4.64	6.12	3.38	6.05	7.38	6.27	6.43	7.02	7.51	6.58	5.23
Fe_2O_3	1.42	1.37	1.24	2.36	0.00	0.69	1.68	1.36	2.03	0.00	3.34	8.23	0.57	4.16	1.34	0.07	0.00	0.45
FeO	17.88	19.16	16.96	17.08	17.89	18.64	17.88	18.61	17.86	17.93	17.20	17.63	19.61	15.57	18.35	19.19	19.08	19.13
MnO	0.29	0.34	0.33	0.33	0.28	0.34	0.30	0.34	0.31	0.27	0.32	0.32	0.37	0.34	0.30	0.36	0.25	0.40
MgO	10.02	9.44	11.56	10.37	11.18	10.21	9.34	10.38	10.36	11.51	10.24	9.79	9.57	10.73	9.88	9.29	9.71	10.37
CaO	12.33	11.93	11.94	12.43	12.24	12.24	12.15	12.61	11.98	12.09	12.11	9.47	12.20	12.28	12.17	12.16	12.30	11.48
Na_2O	0.90	0.73	0.51	0.58	0.86	0.92	0.95	0.57	0.63	0.73	0.64	0.48	0.61	0.44	0.79	1.07	0.77	0.43
K_2O	0.25	0.32	0.16	0.25	0.30	0.26	0.36	0.29	0.25	0.10	0.26	0.23	0.34	0.11	0.25	0.39	0.35	0.24
total	98.33	99.23	97.74	96.95	97.80	98.53	97.30	98.94	98.22	97.09	98.23	98.74	98.74	98.32	98.36	97.39	97.63	97.37
Si	7.120	7.089	7.386	7.305	7.447	7.233	6.994	7.401	7.224	7.596	7.144	6.777	7.283	7.118	7.158	7.110	7.258	7.427
Al	.880	.911	.614	.695	.552	.768	1.006	.599	.776	.404	.856	1.223	.718	.882	.842	.890	.742	.573
Al	.382	.447	.249	.193	.284	.347	.439	.210	.297	.190	.208	.084	.380	.239	.388	.446	.420	.349
Ti	.017	.021	.026	.008	.011	.015	.015	.010	.011	.019	.019	.012	.017	.017	.015	.024	.016	.001
Fe^{3+}	.158	.152	.138	.268	.000	.007	.190	.151	.227	.000	.375	.930	.064	.463	.150	.008	.000	.051
Fe^{2+}	2.223	2.368	2.101	2.153	2.221	2.313	2.255	2.301	2.221	2.237	2.146	2.215	2.434	1.926	2.282	2.422	2.390	2.394
Mn	.037	.043	.041	.042	.035	.043	.038	.043	.039	.034	.040	.041	.047	.043	.038	.046	.032	.051
Mg	2.220	2.080	2.552	2.329	2.473	2.258	2.099	2.288	2.296	2.559	2.276	2.192	2.118	2.366	2.189	2.089	2.168	2.313
Ca	1.964	1.890	1.895	2.007	1.947	1.947	1.963	1.998	1.909	1.933	1.935	1.525	1.941	1.947	1.939	1.966	1.974	1.841
Na	.259	.209	.147	.170	.248	.265	.278	.163	.182	.211	.185	.140	.176	.126	.228	.313	.224	.125
K	.047	.060	.030	.048	.057	.049	.069	.055	.047	.019	.050	.044	.064	.021	.047	.075	.067	.046

amphibole. A location map of the microprobe spot analyses compiled in composition derived from these data is given in Table 1

35	37	38	39	40	41	42	43	44	45	46	47	48	49	50	51
42.66	43.38	46.04	43.78	43.70	43.06	44.99	45.37	43.36	42.46	44.59	45.07	43.74	43.74	46.48	44.44
1.19	1.08	0.59	1.14	1.18	1.11	0.79	0.88	1.16	1.17	1.01	0.93	1.09	1.05	0.77	1.19
11.84	10.57	8.54	11.47	12.06	12.35	10.05	10.00	11.77	12.50	10.88	10.98	12.09	11.98	9.27	11.71
0.00	0.20	0.86	0.00	0.00	0.00	0.00	0.00	0.00	0.00	0.00	0.00	0.00	0.00	0.00	0.00
20.38	20.00	19.71	20.02	19.52	19.15	20.64	19.49	18.65	19.69	20.14	19.52	19.68	19.72	19.55	19.55
0.34	0.36	0.40	0.28	0.28	0.29	0.32	0.29	0.24	0.36	0.29	0.31	0.32	0.29	0.32	0.30
7.21	8.33	8.92	7.85	7.63	7.98	7.63	8.21	7.27	7.60	7.80	7.83	7.68	7.72	8.17	7.85
11.21	11.12	11.49	11.04	11.00	11.12	10.76	10.75	11.09	10.95	11.11	11.31	11.13	11.11	11.11	10.98
1.30	1.35	0.99	1.38	1.54	1.25	1.23	1.28	1.51	1.56	1.29	1.29	1.48	1.65	1.09	1.38
0.96	0.86	0.52	0.93	0.94	0.91	0.79	0.79	1.00	1.01	0.77	0.89	0.91	0.95	0.69	0.91
97.09	97.25	98.06	97.90	97.85	97.22	97.20	97.06	96.05	97.30	97.88	98.13	98.12	98.21	97.45	98.31
6.541	6.629	6.932	6.624	6.599	6.538	6.850	6.875	6.653	6.477	6.734	6.769	6.592	6.593	7.001	6.665
1.459	1.371	1.068	1.376	1.401	1.462	1.150	1.125	1.347	1.523	1.266	1.231	1.408	1.407	1.000	1.335
.681	.533	.448	.670	.746	.748	.653	.661	.782	.725	.671	.713	.740	.721	.647	.735
.137	.124	.067	.130	.134	.127	.091	.100	.134	.134	.115	.105	.124	.119	.087	.134
.000	.023	.097	.000	.000	.000	.000	.000	.000	.000	.000	.000	.000	.000	.000	.000
2.613	2.556	2.482	2.535	2.465	2.432	2.628	2.470	2.393	2.512	2.544	2.452	2.480	2.486	2.463	2.452
.044	.047	.051	.036	.036	.037	.041	.037	.031	.047	.037	.039	.041	.037	.041	.038
1.648	1.897	2.002	1.770	1.717	1.806	1.731	1.854	1.662	1.728	1.756	1.753	1.725	1.734	1.834	1.755
1.842	1.821	1.854	1.790	1.780	1.809	1.755	1.745	1.823	1.790	1.798	1.820	1.797	1.794	1.793	1.764
.387	.400	.289	.405	.451	.368	.363	.376	.449	.461	.378	.376	.433	.482	.318	.401
.188	.168	.100	.180	.181	.181	.153	.153	.196	.197	.148	.171	.175	.183	.133	.174

Table 4. Chemical analyses of a biotite grain with cracks containing secondary minerals

	1	2	3	4	5	6	7	8	9	10	11	12
SiO_2	35.64 (0.22)	35.27	35.34	35.16	35.35	35.32	35.88	44.83	48.57	35.07	47.36	34.69
Al_2O_3	18.19 (0.18)	18.09	17.71	18.33	17.69	18.52	18.41	30.91	34.32	18.46	33.92	18.52
TiO_2	4.19 (0.14)	3.73	3.71	3.39	2.89	3.07	2.66	3.16	1.36	1.63	2.04	1.04
FeO	20.85 (0.31)	21.19	22.20	21.49	22.32	21.13	21.71	5.21	0.91	23.51	0.82	24.51
MgO	7.14 (0.45)	7.04	7.32	7.00	7.83	7.38	7.85	1.89	0.41	7.73	0.59	8.71
MnO	0.21 (0.07)	0.16	0.11	0.29	0.15	0.16	0.20	-	-	0.19	-	0.20
CaO	-	-	-	-	-	-	0.05	-	-	0.05	-	0.06
Na_2O	0.13 (0.04)	0.13	0.04	0.07	0.02	0.04	0.10	0.18	0.14	0.04	0.26	0.16
K_2O	9.50 (0.18	9.76	9.63	9.63	9.46	9.72	9.47	9.63	8.75	9.21	10.25	7.75
	95.87 (0.54	95.37	96.06	95.41	95.71	95.34	96.33	95.81	94.46	95.89	95.24	95.64
Si	5.437 (0.047)	5.428	5.421	5.419	5.441	5.426	5.461	6.067	6.400	5.409	6.271	5.355
Al IV	2.563 (0.047)	2.572	2.579	2.581	2.559	2.574	2.539	1.933	1.600	2.591	1.729	2.645
	8.000	8.000	8.000	8.000	8.000	8.000	8.000	8.000	8.000	8.000	8.000	8.000
Al VI	0.707 (0.050)	0.709	0.622	0.747	0.650	0.779	0.764	2.996	3.729	0.765	3.564	0.723
Ti	0.481 (0.014)	0.432	0.428	0.393	0.335	0.355	0.304	0.322	0.135	0.189	0.203	0.121
Fe	2.660 (0.047)	2.727	2.848	2.770	2.873	2.715	2.764	0.590	0.100	3.033	0.091	3.164
Mg	1.622 (0.095)	1.615	1.674	1.608	1.796	1.690	1.781	0.381	0.081	1.777	0.116	2.004
Mn	0.031 (0.011)	0.021	0.014	0.038	0.020	0.021	0.021	-	-	0.025	-	0.026
	5.501	5.504	5.585	5.556	5.673	5.558	5.638	4.289	4.044	5.786	3.974	6.038
Ca	-	-	-	-	-	-	0.008	-	-	0.008	-	0.010
Na	0.039 (0.013)	0.039	0.012	0.021	0.006	0.012	0.030	0.047	0.036	0.012	0.067	0.048
K	1.848 (0.032)	1.916	1.884	1.893	1.857	1.905	1.839	1.662	1.471	1.812	1.731	1.526
	1.887	1.955	1.896	1.914	1.863	1.916	1.876	1.710	1.506	1.832	1.798	1.584

1. Average of five analyses from the centre of a primary biotite grain. Figures in parentheses represent one standard deviation. 2, 3. Biotite parent grain 200 μm from cracks. 4, 5. Biotite parent grain 15 μm from cracks. 6, 7. Biotite parent grain at leading edge of cracks. 8, 9. Secondary high-Ti muscovite co-existing with ilmenite in crack. 10. Average of three analyses of secondary recrystallised pale biotite at the margin of the parent grain. 11. Secondary muscovite co-existing with secondary biotite at margin of parent grain. 12. Secondary biotite growing in microfractures.